Biogenic Fabrication of Iron and Zinc using Carob Seed Extract and their Antibacterial Activity

Zahrra Hamza Farhan[1], Atheer Saieb Naji Al-Azawey[2*]

[1] Environmental Pollution Department, College of Environmental Sciences, Al-Qasim Green University, Babylon 51013, Iraq

* Corresponding author's email: atheersaieb@environ.uoqasim.edu.iq

ABSTRACT

Biogenic synthesis of iron and zinc nanoparticles from carob seed extract (*Ceratonia siliqua* L.) and their antibacterial activity were studied. The characteristics of the prepared nanoparticles were evaluated shapes and sizes by field emission scanning electron microscopy (FESEM) analysis with mapping technique and energy dispersive X-ray analysis (EDX), and Fourier-transform infrared spectroscopy (FTIR) confirmed the functional group that contributes to the biogenic and antibacterial activity. The appearance of metal-oxygen bonds for both ZnO NPs and Fe_2O_3 NPs in spectra and the presence of zinc, iron, and oxygen in varying proportions confirm the success of the biosynthesis of the nanoparticles. *Ceratonia siliqua* L. extract, iron, and zinc showed high effectiveness in removing bacteria from polluted water.

Keywords: *Ceratonia siliqua* L., antibacterial activity, biosynthesis, zinc, iron.

INTRODUCTION

Microbial contamination is one of the most critical aspects of water contamination, especially pathogenic bacteria such as enteric pathogens, which are often the cause of waterborne diseases. Water pollution is also a serious environmental problem as it has rapid and significant negative impacts on human health and the biodiversity of aquatic ecosystems (Karaboze et al., 2003). Due to the abuse of antibacterial drugs, microorganisms have become resistant to a variety of antibiotics, which has brought great difficulties to the treatment of infectious diseases. Given the increasing resistance of many microorganisms to the currently used antimicrobial agents, as well as the high cost and some adverse effects of synthetic compounds, there is a need to find alternatives (Davies, 1994). The combined impact of antibiotics found in plant extracts towards the bacteria that are resistant to drugs presents new possibilities for the treatment of infectious illnesses and establishes the plant as a viable candidate for the creation of drugs (Fabricant et al., 2003). For centuries, plants have been considered an important source of medicinal compounds, and many unique pharmaceutical ingredients are derived from natural plant sources. Traditionally, many of these plants and their extracts have been used medicinally. Plants are rich in secondary metabolites with antibacterial effects, such as tannins, terpenoids, alkaloids and flavonoids (Obeidat et al., 2012). Plant-mediated nanoparticle synthesis has attracted widespread attention due to its inherent advantages, such as speed, simplicity, environmental friendliness, and low cost (Raheem et al., 2018). Nanotechnology is a branch of nanoscience that studies the synthesis and control of nanoscale substances (Mude et al., 2018).

Generally, between 1 nm and 100 nm, engineered nanomaterials have appeared in a variety of fields such as food, agriculture and medicine. The size of nanoparticles (NPs), does not exceed 100 nm. One can also see properties unique to physical processes at micro scales: tiny webbing, large surface area/volume ratios. In addition,

particles that would not be a metal in bulk can act as if they emit electric currents, and pseudo metallic semiconducting materials able to provide a newly boosting catalyst for reactions are also found here. Highly directional thermal conduction and refraction with large difference between refractive indices can be observed only under such conditions (Tabrez et al., 2016; Venkatesan et al., 2020). Specifically, the heightened responsiveness of the property prompts inquiry into the possible hazardous hazard it poses to human and environmental health, as well as the surroundings that contribute to this toxicity (Dimkpa, 2014; 2018). Hence, the production of nanoparticles using biosynthesis has emerged as a favored approach due to its enhanced safety, cost-effectiveness, biocompatibility, and eco-friendliness in comparison to chemically manufactured nanoparticles (Rao, 2016).

There are multiple stages of iron oxides, such as hematite (α-Fe_2O_3), maghemite (γ-Fe_2O_3), goethite (α-FeOOH), and magnetite (Fe_3O_4). The size scale has a strong effect on the optical, electrical properties and biocompatibility of these materials (Ajinkya et al., 2020; Kudr et al., 2017).

The surface charge of iron oxide particles is also influenced by the functional groups of the coating data, so that their biological activity is affected directly in consequence (Feng et al., 2018). The size of the particles, their surface chemistry and level of dispersion all govern how iron oxides behave in aqueous phases in the environment, according to new research by HU Izhongwen regional university Research Student Yang Jianguo reported past summer. These attributes are all important because of how intimately they interact and combine with an ever-changing mix of different fine chemicals (Li et al., 2014). As an example, iron oxide nanoparticles have the potential to inhibit bacteria from proliferating due their vast surface area and X-ray diffraction patterns with many faces and corners. In addition, new research shows novel mechanisms of ion capture by iron for the first time (Thukkaram et al., 2014).

With a variety of plant parts such as their roots, leaves, stems, seeds, buds, or fruits, such resources can be used to bio-synthesize zinc oxide nanoparticles. These nanoparticles exhibit different phytochemical properties and activities across the plant kingdom (Pradeep et al., 2020). Zinc oxide (ZnO) metal oxide is a semiconductor with n-type conduction. It was known as an important technical material used in plenty of applications from electronics and optics. ZnONP is a semiconductor in its nature, with a 3.37 eV large band gap, and high exciton energy of up to 60 meV. In addition, it has UV-resistant properties which make the substance an excellent optical filter for use in organic photovoltaic cells (Pradeep et al., 2015). Zinc oxide nanoparticles (ZnONPs) have been employed broadly in a number of biomedical fields. They are a widely used material for making implantable programmed drug release capsules, and have been known to function (Elumalai et al., 2015) even in the field known as 'cancer' when applied in its anti-diabetic role; meanwhile they also serve food processing and storage control purposes just as well if the kitchen environment is humid enough (Sangani et al., 2015; Hameed et al., 2016). In addition, ZnONPs have both piezoelectric and thermoelectrical attributes (Nagajyothi et al., 2014).

The Fabaceae family's subfamily is one of the members within it, known scientifically as *Ceratonia siliqua* L. Carob trees can grow to be 12–15 meters in height and live for 100 years. The tree is known for its economic and ecological significance in the Mediterranean basin while growing as far east as Southwest Asia. This perennial tree, which belongs to the jigsaw tree family and is renowned for its hardiness in dry weather, rarely produces fruit. The plant is growing rapidly all over the world and may now be seen without any trouble in Spain, Italy, Tunis and Morocco. The worldwide annual output of carob products exceeds 315,000 tons (Baumel et al., 2018).

Carob pods consist of 90% pulp and 10% seeds. Carob is well-suited to the USDA zones 9–11 in the United States, including Texas, Florida, and Hawaii. Contemporary plant science and agricultural studies often see it as a "neglected" crop in several locations. Carob fruit, flour, and syrup are shown to be abundant when it comes to carbs, proteins, and minerals (Karababa et al., 2013).

Moreover, carob milk is rich in antioxidants and essential nutrients necessary for life. It is 48–56% sugar, primarily composed of the sugars fructose, sucrose, glucose and maltose. It also provides 18% dietary fiber, mainly in the form of cellulose and hemicellulose (Dakia et al., 2003). Pods are a good source of dietary fiber that contains both cellulose (18%) and pectin (18%), and they also provide enough condensed tannins in terms on average about 16–20% (Dakia et al., 2003). The recovery of Fe and Zn in Canob seed extract achieved in this study via a green process can be used for economic improvement as well as an antibacterial agent in modern packaging.

EXPERIMENTAL PART

Biosynthesis of FeO nanoparticles

According to the methodology described in (Awad et al., 2014), the preparation steps were as follows. The process of synthesizing iron nanoparticles is as follows: Step 1: Weighting between 1 and 10 grams of carob pod pieces were immersed in ultrapure water 150 ml for a duration amounting to two hours. Step 1–2: A solution containing 2–3.8 grams of ferric chloride (FeCl$_3$·6H$_2$O) was prepared by dissolving it in 100 milliliters of ultrapure water for a duration amounting to 15 minutes. Step 3: The precursor iron solution was combined with the extract in a 1:1 volume ratio. The addition of the plant extract in ultrapure water containing ferric chloride as precursor meant that what had been a yellowish hue became brown, is indicative of iron nanoparticles having formed in the solution. Step 4: the browned-black powder of graphene-based iron oxide nanoparticless (gIONPs) and its antibacterial activity were used.

Biosynthesis of ZnO nanoparticles

The preparation was executed in accordance with the prescribed procedure. The process of biosynthesis of ZnO nanoparticles involves five main steps:

1. The pods of the carob tree (*C. siliqua* L.) were air-dried for a period of one month at room temperature
2. Afterwards, the pods were mechanically crushed using a kibbler and then separated from the seeds. The seeds were then pulverized into a fine powder using a mixer.
3. A quantity of 3–5–10 grams of the pod powder was introduced into distilled water and heated at 60 degrees Celsius for a duration of 1 hour.
4. A 100 mL volume of plant broth was combined with 0.1 M zinc acetate dehydrate at a ratio of volume to volume.
5. The bio-ZnONPs that were generated were gathered using centrifugation at a force of 8000 times the acceleration due to gravity for a duration of 10 minutes.

Antibacterial activity test

The process of antibacterial activity test involves five main steps:

1. 0.1, 0.5, 1 g has been weighed as powder for each of ZnONPs and Fe$_2$ONPs.
2. Add each of these weight to 100 ml of waste water and shaking using magnetic stirrer for 15 minutes to allow bacteria to contact with NPs.
3. The NPs were remained in wastewater for 24 h under laboratory conditions.
4. 1 ml of treated waste water were taken from each concentration 0.1, 0.5, 1 g/100 ml for each nanoparticle of ZnO and Fe$_2$O, then serial dilutions were made and appropriate dilution was chosen to culture bacteria on nutrient and macconkey agar and incubated at 37 °C for 24 h, this step was repeated in triplicate.
5. The colonies of bacteria which grow on nutrient and macconkey agar were calculated manually, the removal efficiency can be calculated by %RE (removal efficiency) = N1–N2/N1, where N1 and N2 denote the number of colonies before and after treatment.

RESULTS AND DISCUSSION

Fourier-transform infrared spectroscopy

Fourier-transform infrared spectroscopy (FTIR) is a straightforward analytical method employed to determine the presence of functional groups in solid nanoparticles. FTIR spectrum of the carob plant (*C. siliqua* L.) is shown in Figure 1. The spectrum showed a broad absorption peak at 3436 cm^{-1} attributed to free hydroxyl groups due to the presence of oleic acids. In turn, the absorption peak at 2073 cm^{-1} is due to the stretching vibration of unbound CO. The absorption peaks seen at 1637, 1076, and 692 cm^{-1} are a result of the intense stretching of the C=O bond in the carbonyl group, the stretching vibration of C-N functional groups in plant polyphenolic species, and the stretching of the C-S bond, respectively (Demirezen et al. 2022). Figure 2 shows the FTIR spectrum of ZnO nanoparticles biosynthesized using the C. siliqua plant. It was observed from the spectrum that clear absorption peaks appeared at 3412, 2924, 1733, and 1621 cm^{-1} assigned to stretching vibration of O-H, C-H, and C=O groups, respectively. In turn, the last absorption peaks are 1621, 1437, 1369, 1230, 1104, 755, and 626 cm^{-1} assigned to C=C, N–O, bending C-H, C=N, C-OH, bending C=C, and Zn-O, respectively (Karmous et al., 2022). On the other hand, the FTIR spectrum of Fe$_2$O$_3$ nanoparticles showed a broad absorption
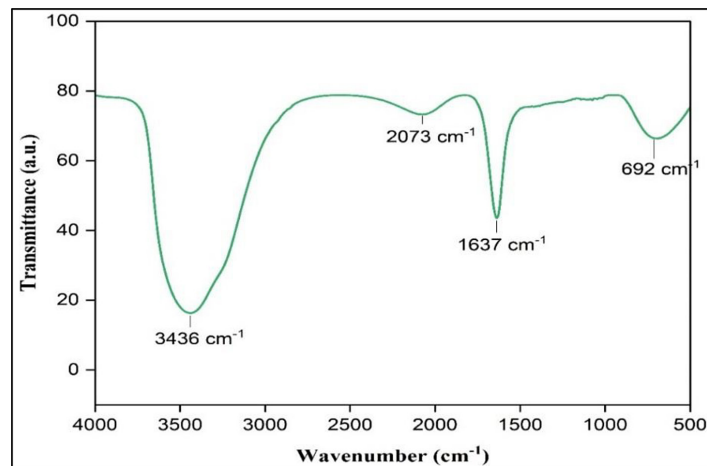
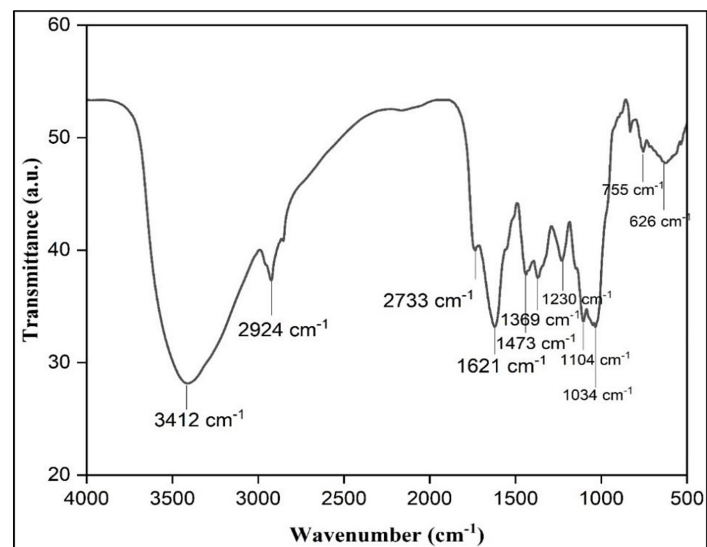**Figure 1.** FTIR spectrum of *C. siliqua* L.

Figure 2. FTIR spectrum of ZnO NPs

peak at 3372 cm^{-1} assigned to the O-H stretching vibration of the hydroxyl groups. The absorption peaks at 2925, 1615, 1380, 1099, 1023, and 695 cm^{-1} are due to C-H, C=C, bending C-H, C–O–C, C-N, and Fe-O stretching, respectively (Farahmandjou and Soflaee 2015) (Table 1).

Field emission scanning electron microscopy analysis

FESEM is an important technique that reveals the morphology, size, and crystalline nature of the prepared nanocomposites. Figure 4, FESEM analysis of *C. siliqua* L., illustrates a recently polished steel surface that is exceptionally smooth and devoid of corrosion, albeit with minor flaws resulting from the polishing process. EDX spectrum showed the presence of several elements:

carbon (47.91%), nitrogen (6.34%), oxygen (30.61%), chloride (4.95%), potassium (8.27%), and arsenic (1.92%). This indicates the presence of compounds in the content of the *C. siliqua* L., which are luteolin-7-glucoside, followed by epi-catechin, apigenin-7-glucoside, quercetin-3-O-glucoside, caffeic acid, gallic acid, and chlorogenic acid (Dahmani et al. 2023). Figure 5 shows the FESEM analysis of biosynthesized zinc oxide nanoparticles. The FESEM image of biosynthesized ZnO NPs reveals a densely arranged layered structure, with each layer being stacked in a layer. The EDX analysis sand elemental mapping, which is displayed in Figure 5b, verified that metallic zinc oxide was present in the biosynthesized ZnO NPs. According to the EDX study, the composition was carbon (49.45%), oxygen (42.52%), and zinc (8.03%). The high amounts

Table 1. FTIR characterization for prepared nanoparticles

Sample	Wavenumber (cm^{-1})	Functional group
ZnO	3412.59	Stretching vibration of O-H
	2924.65	Stretching vibration of C-H
	1733.47	Stretching vibration of C=O
	1621.48	Stretching vibration of C=C
	1437.39	Stretching vibration of N–O
	1369.92	Bending vibration of C-H
	1230.55	Stretching vibration of C=N
	1104.17	Stretching vibration of C-O
	1034.50	Stretching vibration of C − OH
	755.70	Bending vibration of C=C
	626.91	Zn-O
Fe$_2$O$_3$	3372.05	Stretching vibration of O-H
	2925.05	Stretching vibration of C-H
	1615.10	Stretching vibration of C=C
	1380.74	Bending vibration of C-H
	1099.27	Stretching vibration of C–O–C
	1023.64	Stretching vibration of C–N
	695.10	Fe-O stretching
C. siliqua L.	3436.67	Stretching vibration of -OH
	2073.29	Unbound CO
	1637.97	Unsaturated carbonyl groups
	1076.01	C-N function groups
	692.01	C-S stretching
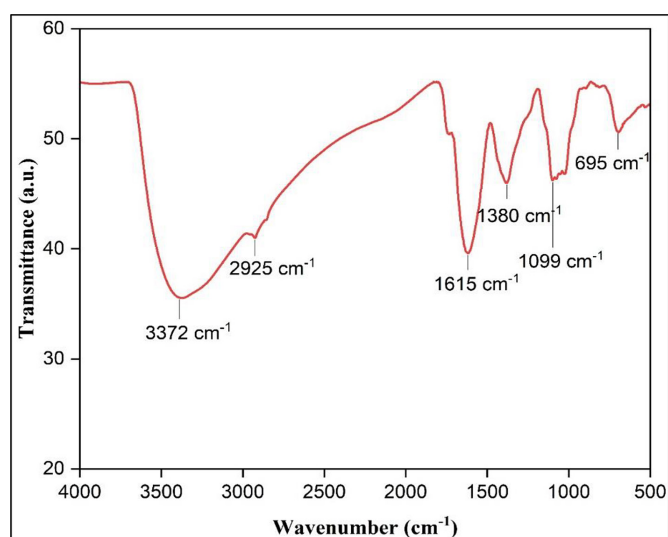
Figure 3. FTIR spectrum of Fe$_2$O$_3$ NPs

of carbon show that plant phytochemical groups are involved in the reduction and capping of the produced ZnO NPs (5). FE-SEM software was utilized to process the image resolution of biosynthesized Fe$_2$O$_3$ nanoparticles, which is depicted in Figure 6. The sample exhibits a not uniform size distribution and a sime-spherical-like morphology, as is readily apparent. The EDX spectra and elemental mapping reveal that the nanoparticles synthesized are primarily composed of Fe (58.31%) and O (24.63%). EDX spectrum (Fig. 4b) demonstrates that molecules, such as carbon (13.37%),
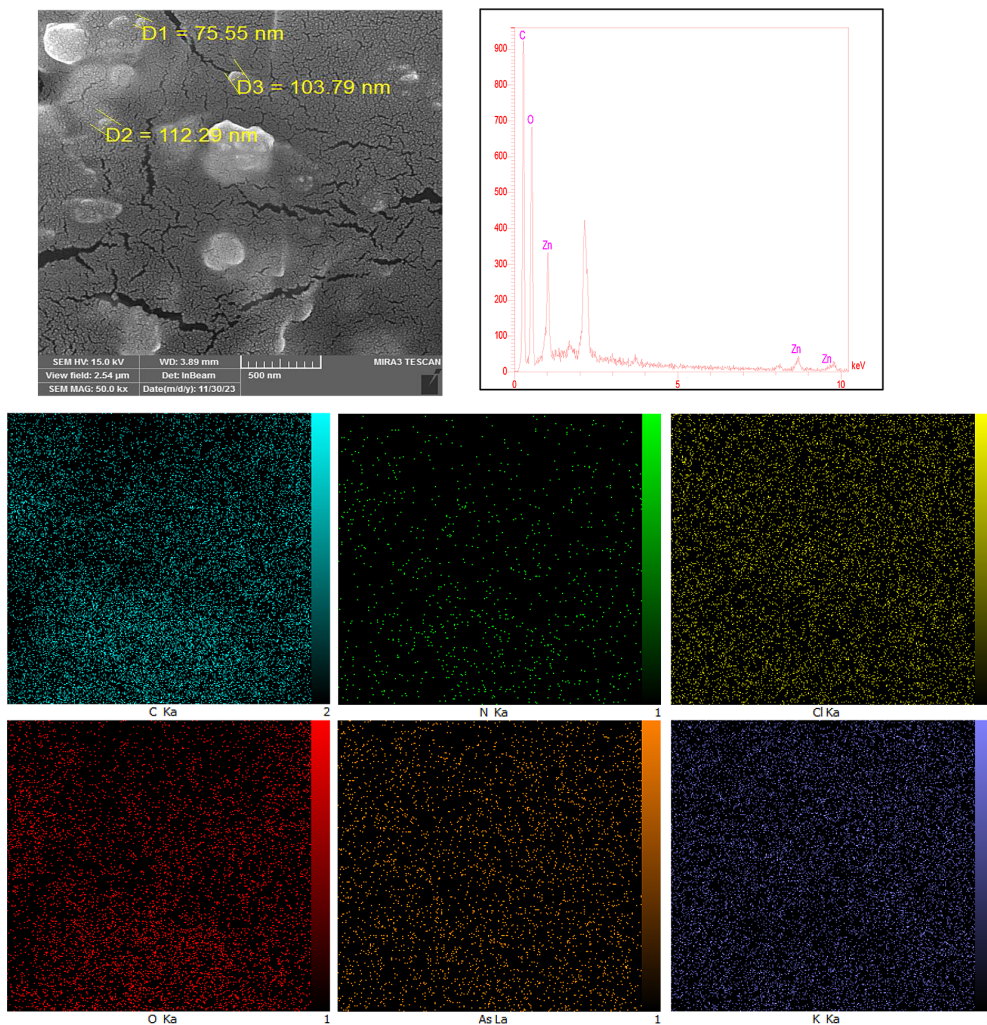
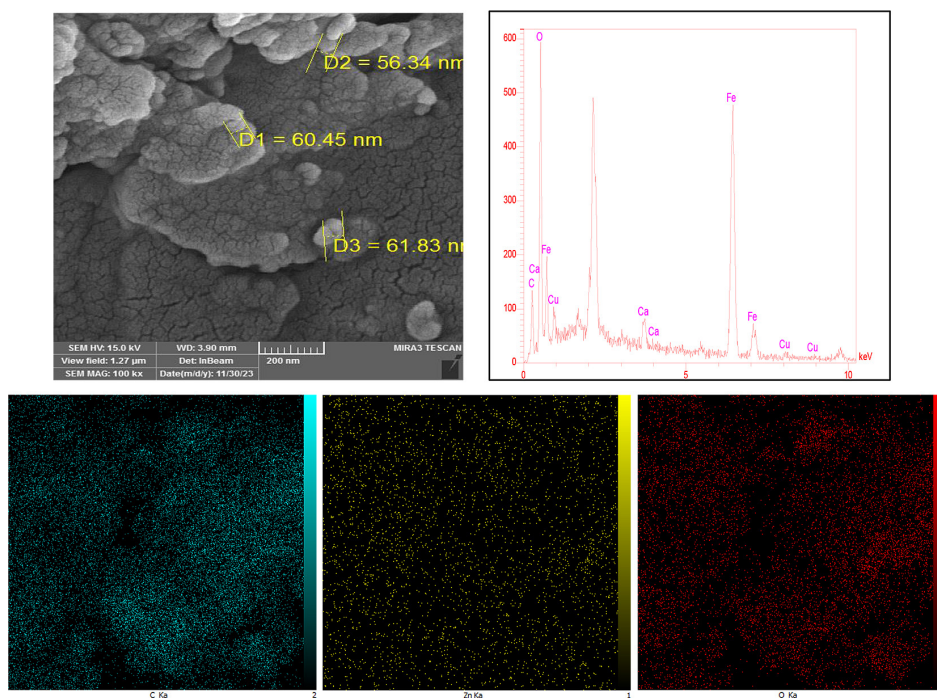**Figure 4. (**a) FE-SEM image, (b) EDX spectrum, and (c) mapping of *C. siliqua* L.

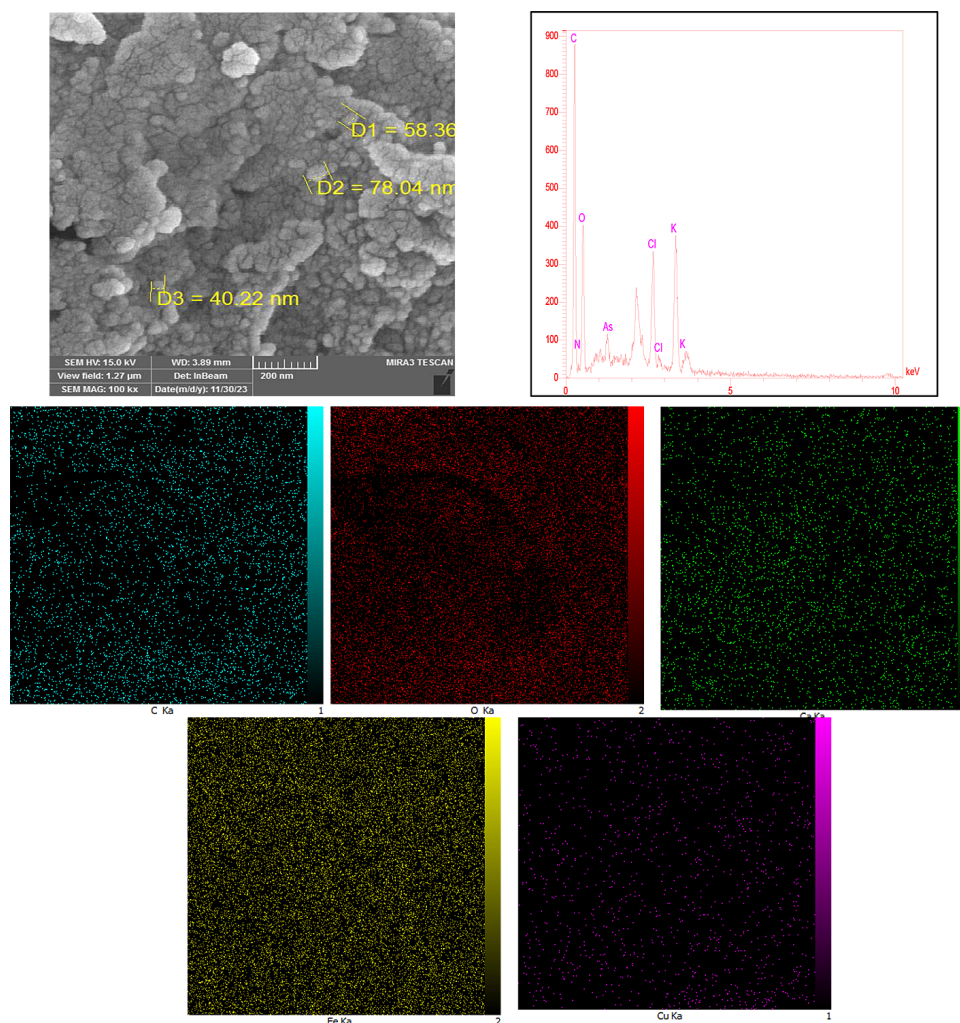**Figure 5. (**a) FE-SEM image, (b) EDX spectrum, and (c) mapping of ZnO NPs

Figure 6. (a) FE-SEM image, (b) EDX spectrum, and (c) mapping of Fe$_2$O$_3$ NPs

calcium (1.94%), and copper (1.75%) are present in the reaction mixture other than Fe nanoparticles; these components interpret the complex of the plant extract

Antibacterial activity study

Antibacterial activity of Carob against the total count of bacteria

Before undergoing treatment, the initial concentration of Carob-negative bacteria stood at 25000 CFU/ml. Following treatment with varying concentrations of Carob (0.1 g/100 mL, 0.5 g/100 mL, and 1 g/100 mL), as depicted in Figure 7, notable removal efficiencies were achieved. Specifically, removal efficiencies were recorded at 90%, 100%, and 100%, respectively. These findings underscore the efficacy of Carob in mitigating bacterial contamination in wastewater, with higher concentrations exhibiting superior removal rates. The graphical representation in Figure 7 provides a comprehensive visualization of the correlation between Carob concentration and removal efficiency, facilitating the development of tailored treatment strategies for effective bacterial decontamination in wastewater treatment processes.

Antibacterial activity of Carob against gram-negative bacteria

Before treatment, the initial concentration of negative bacteria Carob was identified to be 19400 CFU/ml. Upon treatment with Carob at various concentrations (0.1 g/100 mL, 0.5 g/100 mL, and 1 g/100 mL), as showcased in Figure 8, noteworthy removal efficiencies were observed. Specifically, removal efficiencies were measured at 37%, 100%, and 100%, respectively. This underscores a significant improvement in bacterial removal efficacy with escalating Carob concentration. Notably,
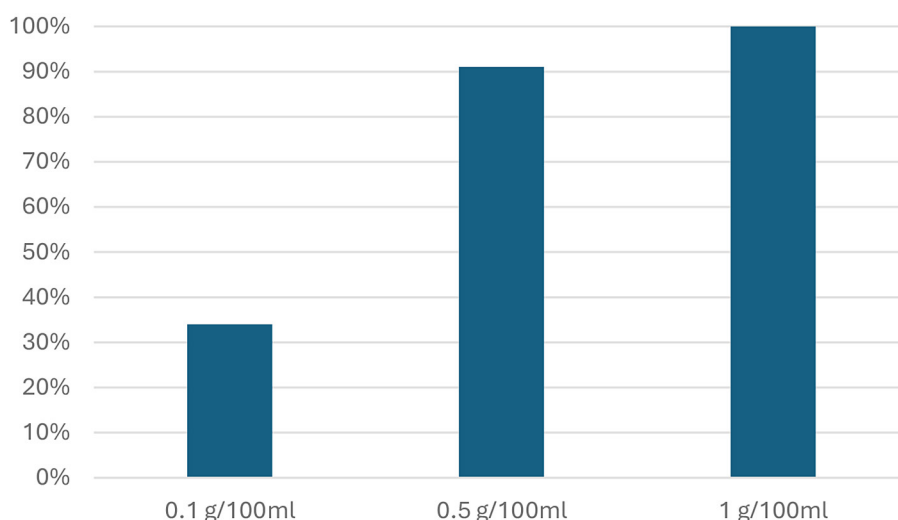
Figure 7. Removal efficiency of Carob against the total count of bacteria
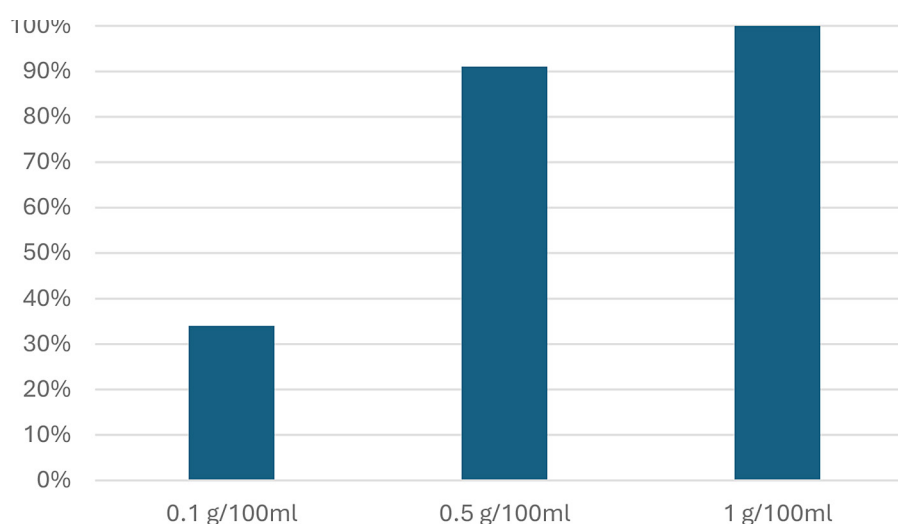

Figure 8. Removal efficiency of Carob against negative bacteria

the complete eradication achieved at concentrations of 0.5 g/100 mL and 1 g/100 mL underscores the potent antibacterial attributes of Carob at higher concentrations. Furthermore, the visual representation in Figure 8 elucidates the relationship between Carob concentration and removal efficiency, facilitating a comprehensive understanding of the treatment effectiveness across varied concentrations.

Antibacterial activity of ZnO NPs against the total count of bacteria

Bacterial pollution of wastewater was tested against the total count of bacteria. The total count of bacteria before treatment with ZnO NPs was 25000 CFU/ml. After treatment, the number of bacterial colonies was decreased where the removal efficiency of the total count of bacteria

was 34%, 91%, and 100% after treatment with different concentrations of nanoparticles was 0.1 g/100 mL, 0.5 g/100 mL, and 1g/100 mL, respectively, as in Figure 9.

Antibacterial activity of ZnO NPS against gram negative bacteria

Before treatment, the initial concentration of negative bacteria ZnO NPS was determined to be 19400 CFU/ml. Following the treatment with ZnO NPS at varying concentrations (0.1 g/100 mL, 0.5 g/100 mL, and 1 g/100 mL), as depicted in Figure 10, notable removal efficiencies were observed. Specifically, the removal efficiencies were recorded as 24%, 100%, and 100%, respectively. This indicates a significant enhancement in bacterial removal effectiveness with increasing ZnO
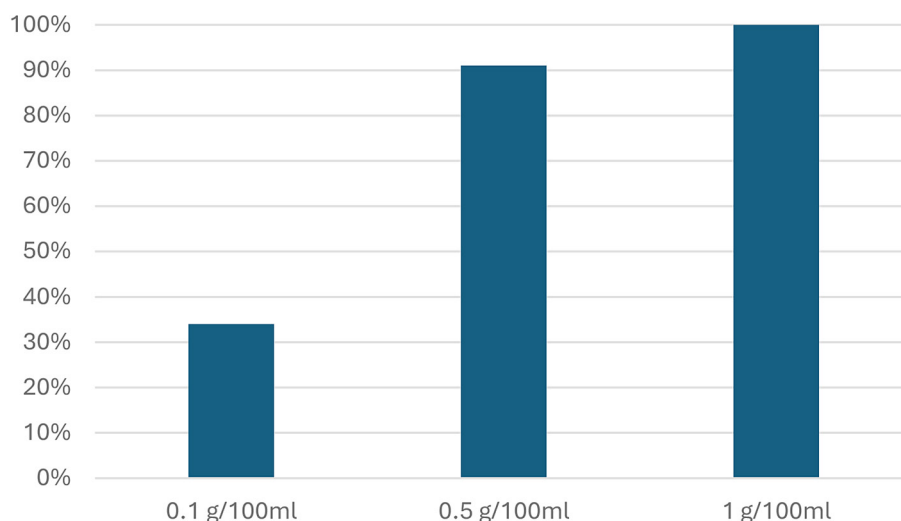
Figure 9. Removal efficiency of ZnO NPs against the total count of bacteria
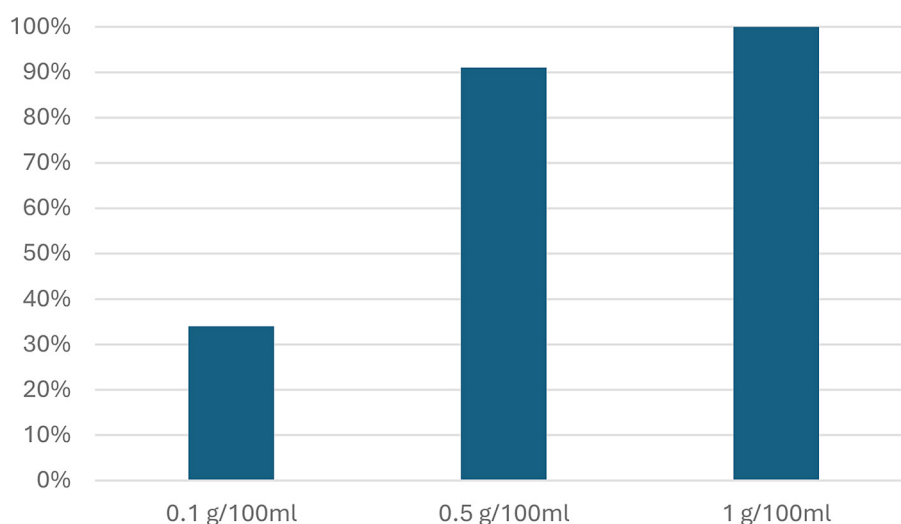

Figure 10. Removal efficiency of ZnO NPS against negative bacteria

NPS concentration. It is noteworthy to highlight the complete eradication achieved with concentrations of 0.5 g/l and 1 g/l, demonstrating the potent antibacterial properties of ZnO NPS at higher concentrations. Additionally, the visual representation in Figure 10 illustrates the correlation between ZnO NPS concentration and removal efficiency, providing a clear understanding of the treatment effectiveness across different concentrations.

Gupta et al. (2017) study on zinc oxide nanoparticles provides further insights into different nanoparticle therapeutics and their effectiveness against bacterial pathogens. Various metal and metal oxide-based nanoparticles, such as silver (Ag), iron (Fe), zinc (Zn), titanium oxide (TiO_2), magnesium oxide (MgO), zinc oxide (ZnO), and iron oxide, along with carbon and graphene-based nanomaterials, are commonly employed as adsorbents, catalysts, and membranes in wastewater treatment. Although the studies differed in terms of nanoparticle compositions and bacterial strains tested, these nanoparticles have proven to be effective in treating wastewater (Anjum et al., 2019; Singh et al., 2019; Baig et al., 2021).

The mechanism of how nanoparticles penetrate bacteria is not fully understood (Adams et al., 2006). When bacteria interact with metal oxide nanoparticles, the shape of the membrane changes. This increases permeability, thereby impairing normal transport across the plasma membrane (Auffan et al., 2009)

Many research works mainly support the idea that in addition to particle size dependence, ZnO nanoparticles also have concentration-dependent antibacterial activity (Jalal et al., 2010).

The antibacterial activity of ZnO nanoparticles can be explained by the interaction of ZnO nanoparticles with bacteria, resulting in the destruction of bacterial surfaces (Zhang et al., 2007).

After zinc oxide disrupts or traps cell membranes, nanoparticles may adhere firmly to the surface of dead bacteria, thereby inhibiting further antimicrobial effects (Yamamoto et al., 2004). This work included the synthesis of zinc oxide nanoparticles (ZnONPs) using carob pods. Experiments were then conducted to show the antibacterial efficacy of the produced nanoparticles (Dimkpa et al., 2022)

The antibacterial activity results of biosynthesized ZnONPs are consistent with other reports on the effectiveness of green synthesized metal oxide nanoparticles, including ZnONPs, as antibacterial agents (Mirzaei et al., 2017; Patel et al., 2015; Sundrarajan et al., 2015; Ifeanyichukwu et al., 2020; Pillai et al., 2020).

The reference is Gupta et al. (2018). ZnONP shown notable antibacterial efficacy against comparable pathogens, such as Staphylococcus aureus MTCC 9760, *Streptococcus pyogenes* MTCC 1926, *Bacillus cereus* MTCC 430, *Pseudomonas aeruginosa* MTCC 424, *Proteus mirabilis* MTCC 3310, and *Escherichia coli* MTCC 40.

The prevalence of medication or agrochemical resistance in human and plant pathogenic bacteria strains has lately escalated. Hence, it is necessary to use other approaches to address microbial infections in biological systems. Recently, there has been a growing importance placed on researching nanomaterials, namely ZnONPs, as potential new antibacterial agents. The findings obtained from the present research add to the ongoing efforts in finding more effective bioantimicrobial and antifungal medicines. Nanoparticles are being increasingly often categorized as antibiotics because of their strong antibacterial properties (Khan et al., 2021).

Antibacterial activity of Fe_2O_3 NPS against the total count of bacteria

The analysis of wastewater for bacterial contamination involved assessing both the total bacterial count and the count of Fe_2O_3 NPS present. Initially, the total bacterial count was determined to be 25000CFU/ml before any treatment. Upon treatment with Fe_2O_3 NPS, a notable removal efficiency of 46% was achieved, indicating a significant reduction in bacterial load. Further investigation involved treating the wastewater with Fe_2O_3 NPS at varying concentrations: 0.1 g/100 mL, 0.5 g/100 mL, and 1 g/100 mL, as depicted in Figure 11. Remarkably, the removal efficiencies observed after treatment at these concentrations were consistently 100%. These were highly effective in killing bacteria even at lower concentrations.

The results of this study emphasize the possible use of Fe_2O_3 nanoparticles (NPs) as a treatment component in water-purification systems, specifically those designed for bacterial pollution. The data presented in Figure 3 show a clear trend: the overall effectiveness of Fe_2O_3 NPs in purifying contaminated water improved alongside increases in the concentration of the NPs themselves.

Antibacterial activity of Fe_2O_3 NPS against Gram negative bacteria

After the initial measurement, the concentration of bacteria (CFU/ml) in the negative control of Fe_2O_3 NPS was established as 19400.
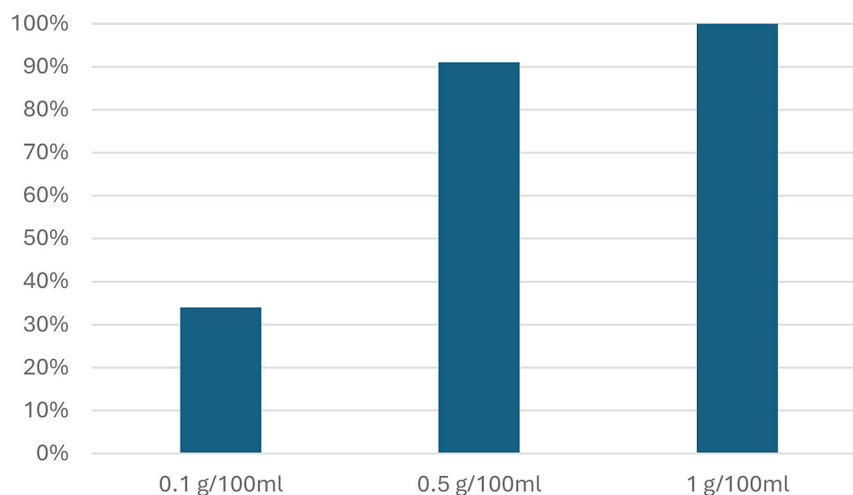

Figure 11. Removal efficiency of Fe_2O_3 NPS against the total count of bacteria

Subsequent treatment of contaminated water with different concentrations of iron oxide nanoparticles (0.1 g/100 mL, 0.5 g/100 mL, and at 1 g/100 mL), as shown in Figure 12, was very efficient. The first concentration of iron oxide led to a 20% removal efficiency while the second batch had a 49% efficiency. Yet, the most impressive result was in the third case: total removal.

The findings make it clear that iron oxide nanoparticles (NPs), especially those with higher concentrations, are very effective at reducing bacterial pollution in wastewater. The impact on bacterial population density is likely due to the absorption of the iron oxide NPs onto the cell surfaces and the ensuing clumping together of the cells. This is shown in the graphical presentation of Figure 4, which highlights the direct relationship between the concentration of Fe_2O_3 NPs and the bacterial removal efficiency of the water treatment process.

The many phases of iron oxides include hematite (α-Fe_2O_3), maghemite (γ-Fe_2O_3), goethite (α-$FeOOH$), and magnetite (Fe_3O_4). The optical, electrical, and biocompatibility characteristics of these materials are influenced by the small scale (Ajinkya et al., 2020; Kudr et al., 2017).

The biological actions of iron oxide nanoparticles is impacted by the functional groups of the coating material, which alter the surface charge (Feng et al., 2018). The dispersion, size, and surface chemistry of iron oxide materials are crucial for aquatic environmental applications because of their porous nature and particle-surface interactions (Li et al., 2014).

Oxidative stress was triggered within nano-size specimens potentially useful in their own right as antibacterial agents owing to their high surface area and crystalline configuration at so many corners and edges by reactive oxygen species (Thukkaram et al., 2014).

Aqueous extract from *C. siliqua* carob pods was employed as a stabilizer, capping agent, and reducing reagent in the preparation of gIONP in this study (Aksu Demirezen et al., 2021).

Because of their simple, economical, and environmentally friendly production methods, green nanomaterials have been the focus of numerous studies on their superior function for traditional antibacterial drugs. Acorus calamus extract. This was the direction of several of these investigations into antibacterial agents (Arasu et al., 2018), copper oxide nanoparticles (Aisida, et al., 2020), and iron oxide nanoparticles made from *Moringa oleifera* leaf extract. Dried shell extract of *Zea mays* L. silver nanoparticles produced using extracts of emblifornia Diffubia (Devi et al., 2020), silver nanoparticles made using piedra cala extract.

According to Mohamed et al. (2015), gIONPs inhibit the generation of reactive oxygen species (ROS) and the oxidative stress brought on by a Fenton reaction.

If iron nanoparticles infiltrate into cells through damaged cell membranes, they will seriously harm them (Li et al., 2018). Iron oxide nanoparticles markedly increased generation of reactive oxygen species such as hydroxyl radicals with bacterial cell death and inhibition of only *E. coli* growth as an additional effect (Table 2). The reaction between atomic oxygen and free radicals leads to the production of types of compounds that treat the pollutants.
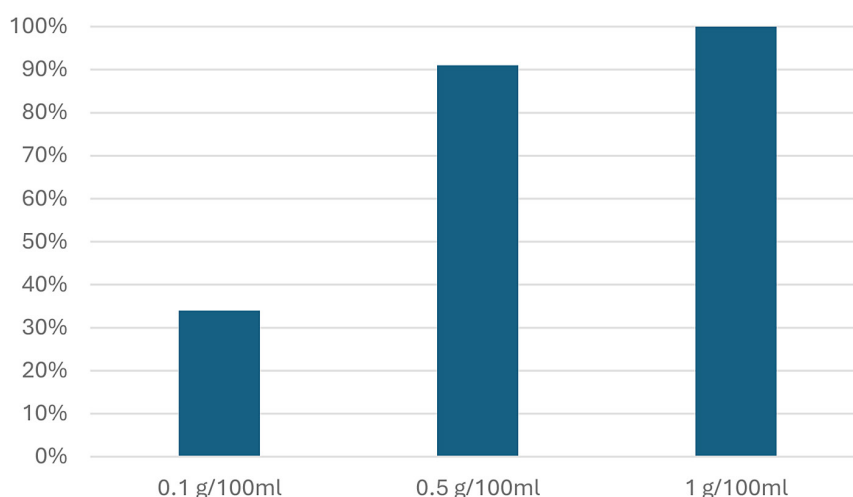

Figure 12. Removal efficiency of Fe_2O_3 NPS against negative bacteria

Table 2. Bacteria removal before and after treatment

Parameter	Before treatment	After treatment								
		ZnO NPs			Fe$_2$O$_3$ NPs			Carab NPs		
Total count of bacteria	25000 CF/mL	0.1g/100ml	0.5g/100ml	1g/100ml	0.1g/100ml	0.5g/100ml	1g/100ml	0.1g/100ml	0.5g/100ml	1g/100ml
		34%	91%	100%	46%	100%	100%	90%	100%	100%
Nagative bacteria	19400 CF/mL	24%	100%	100%	20%	49%	100%	37%	100%	100%

CONCLUSIONS

The zinc oxide and iron oxide nanoparticles were successfully synthesized using carob extract. Green synthesis methods, like this one, are more efficient, cost less, and are currently of higher interest in many different scientific fields. Moreover, when the prepared nanomaterials were used, they demonstrated amazing efficacy in the removal of both positive and negative bacteria from contaminated water.

REFERENCES

1. Aisida S.O., Madubuonu N., Alnasir M.H., Ahmad I., Botha S., Ezema F.I. 2020. Biogenic synthesis of iron oxide nanorods using Moringa oleifera leaf extract for antibacterial applications. Appl. Nanosci., 10, 305−315. https://doi.org/10.1007/s13204-019-01099-x

2. Aisida S.O., Ugwu K., Akpa P.A., Nwanya A.C., Ejikeme P.M., Botha S., Ahmad I., Maaza M., Ezema F.I. 2019. Biogenic synthesis and antibacterial activity of controlled silver nanoparticles using an extract of Gongronema Latifolium. Mater. Chem. Phys., 237, 121859. https://doi.org/10.1016/j.matchemphys 2019.121859

3. Aisida S.O., Ugwu K., Akpa P.A., Nwanya A.C., Nwankwoa U., Botha S.S., Ejikeme P.M., Ahmad I., Maaza M., Ezema F. 2019 Biogenic synthesis and antibacterial activity of controlled silver nanoparticles using an extract of Gongronema Latifolium. I. Surface. Interfac., 17, 100359. https://doi.org/10.1016/j surfin.2019.100359

4. Ajinkya N., Yu X., Kaithal P., Luo H., Somani P., Ramakrishna S. 2020. Magnetic Iron Oxide Nanoparticle (IONP) Synthesis to Applications: Present and Future. Materials, 4644, 13. https://doi.org/10.3390/ma13204644

5. Demirezen D. A., Yılmaz D.D. 2021. Real-time colorimetric detection of dissolved carbon dioxide using pH-sensitive indicator based on anthocyanin and PVA coated green iron oxide nanoparticles at room temperature. Inorg. Nano-Met. Chem. 52, 761−771. https://doi.org/10.1080/24701556.2021.1980032

6. Ali-Shtayeh M.S., Jamous R.M., Al-Shafie' J.H., El-gharabah W.A., Kherfan F.A., Qarariah K.H., Khdair I.S., Soos I.M., Musleh A.A., Isa B.A. 2008. Traditional knowledge of wild edible plants used in Palestine (Northern West Bank): A comparative study. Journal of Ethnobiology and Ethnomedicine 4, 1–13.

7. Anbuvannan M., Ramesh M., Viruthagiri G., Shanmugam N., Kannadasan N. 2015. Synthesis, characterization and photocatalytic activity of ZnO nanoparticles prepared by biological method, Spectrochim. Acta A Mol. Biomol. Spectrosc., 143, 304–308.

8. Arasu M.V., Arokiyaraj S., Viayaraghavan P., Kumar T.S.J., Duraipandiyan V., Al-Dhabi N.A., Kaviyarasu K.J. 2019. One step green synthesis of larvicidal, and azo dye degrading antibacterial nanoparticles by response surface methodology. Photochem. Photobiol. B Biol., 190, 154−162. https://doi.org/10.1016/j.jphotobiol.2018.11.020

9. Balogun S., Ayangbenro A., Ogunsanya G., Azeez A., Muonaka C., Ihongbe M. 2016. Bacteriological pollution indicators in Ogun River flowing through Abeokuta metropolis. Journal of Science and Technology (Ghana), 36, 54–63.

10. Baumel A., Mirleau P., Viruel J., Kharrat M.B.D., La Malfa S., Ouahman L., Diadema K., Moakhar M., Sanguin H., Médail F. 2018. Assessment of plant species diversity associated with the carob tree (*Ceratonia siliqua*, *Fabaceae*) at the Mediterranean scale. Plant Ecol. Evol., 151, 185–193.

11. Dahmani W., Elaouni N., Abousalim A., Akissi Z.L.E, Legssyer A, Ziyyat A, Sahpaz S. 2023. Exploring carob (*Ceratonia siliqua* L.): A comprehensive assessment of its characteristics, ethnomedicinal uses, phytochemical aspects, and pharmacological activities. Plants 12, 3303.

12. Dakia P.A., Wathelet B., Paquot M. 2007. Isolation and chemical evaluation of carob (*Ceratonia siliqua* L.) seed germ. Food Chem., 102, 1368–1374.

13. Davies J. 1994. Inactivation of antibiotics and the dissemination of resistance genes. Science, 264(80), 5157, 375–382.

14. Demirezen D.A., Yılmaz Ş., Yılmaz D.D., Yıldız Y.Ş. 2022. Green synthesis of iron oxide nanoparticles using *Ceratonia siliqua* L. aqueous extract: Improvement of colloidal stability by optimizing synthesis parameters, and evaluation of antibacterial

activity against Gram-positive and Gram-negative bacteria. Int. J. Mater. Res 113, 849–861.

15. Elumalai K., Velmurugan S. 2015. Green synthesis, characterization and antimicrobial activities of zinc oxide nanoparticles from the leaf extract of Azadirachta indica. Appl. Surf. Sci., 345, 329–336.

16. Fabricant D.S. and Farnsworth N.R. 2001. The value of plants used in traditional medicine for drug discovery. Environ. Health Perspect., 109(1), 69–75.

17. Farahmandjou M., Soflaee F. 2015. Synthesis and characterization of α-Fe$_2$O$_3$ nanoparticles by simple co-precipitation method. Physical Chemistry Research, 3, 191–196.

18. Feng Q., Liu Y., Huang J., Chen K., Huang J., Xiao K. 2018. Uptake, distribution, clearance, and toxicity of iron oxide nanoparticles with different sizes and coatings. Sci. Rep., 2082, 1−13. https://doi.org/10.1038/s41598-018-19628-z

19. Gupta M., Tomar R.S., Kaushik S., Mishra R.K., Sharma D. 2018. Effective antimicrobial activity of green ZnO nano particles of Catharanthus roseus. Front. Microbiol., 9, 2030.

20. Hameed A.S., Karthikeyan C., Ahamed A.P., Thajuddin N., Alharbi N.S., Alharbi S.A., Ravi G. 2016. In vitro antibacterial activity of ZnO and Nd doped ZnO nanoparticles against ESBL producing *Escherichia coli* and *Klebsiella pneumoniae*. Sci. Rep., 6, 24312.

21. Ifeanyichukwu U.L., Omolola E.F., Collins N.A. 2020. Green synthesis of zinc oxide nanoparticles from Pomegranate (*Punica granatum*) extracts and characterization of their antibacterial activity. Molecules, 25, 4521.

22. Karababa E., Coşkuner Y. 2013. Physical properties of carob bean (*Ceratonia siliqu*a L.): An industrial gum yielding crop. Ind. Crops Prod., 42, 440–446.

23. Karaboze I., Ucar F., Eltem R., Ozdmir G., and Ate M.S., 2003. Determination of existence and count of pathogenic microorganisms in Izmir Bay, JES, 26, 1–18.

24. Karmous I., Taheur F.B., Zuverza-Mena N., Jebahi S., Vaidya S., Tlahig S., Mhadhbi M., Gorai M., Raouafi A., Debara M. 2022. Phytosynthesis of zinc oxide nanoparticles using *Ceratonia siliqua* L. and evidence of antimicrobial activity. Plants, 11, 3079.

25. Khan M., Khan A.U., Bogdanchikova N., Garibo D. 2021. Antibacterial and antifungal studies of biosynthesized silver nanoparticles against plant parasitic nematode Meloidogyne Incognita, plant pathogens *Ralstonia Solanacearum* and *Fusarium Oxysporum*. Molecules, 26, 2462.

26. Koivunen J., Siitonen A., Heinonen-Tanski H. 2003. Elimination of enteric bacteria in biological–chemical wastewater treatment and tertiary filtration units. Water Research, 37, 690–698.

27. Kudr J., Haddad Y., Richtera L., Heger Z., Cernak M., Adam V., Zitka O. 2017. Magnetic Nanoparticles: From Design and Synthesis to Real World Applications. Nanomaterials, 7(9), 243. https://doi.org/10.3390/nano7090243

28. Li W., Liu D., Wu J., Kim C., Fortner J.D. 2014. Aqueous Aggregation and surface deposition processes of engineered superparamagnetic iron oxide nanoparticles for environmental applications environ. Sci. Technol., 48, 11892−11900. https://doi.org/10.1021/es502174p

29. Li Y., Yang D., Wang S., Li C., Xue B., Yang L., Shen Z., Jin M., Wang J., Qiu Z. 2018 Ultrathin polyamide nanofiltration membranes with tunable chargeability for multivalent cation removal. Molecules, 23, 602. https://doi.org/10.3390/molecules23030606

30. Mohamed Y.M., Azzam A.M., Amin B.H., Safwat N.A. 2015. Mycosynthesis of iron nanoparticles by Alternaria alternata and its antibacterial activity. Afr. J. Biotechnol., 14, 1234−1241. https://doi.org/10.5897/ AJB2014.14286

31. Zehab M.M.P., Shariati-Sharifi F., Jamshidian A., Hajinezhad M.R. 2018. The effect of Syrian mesquite (*Prosopis farcta*) seed extract on thioacetamide-induced oxidative stress in rats. Feyz Medical Sciences Journal, 22, 25–30.

32. Mude N., Ingle A., Gade A., and Rai M. 2009. Synthesis of silver nanoparticles using callus extract of Carica papaya-a first report. J. Plant Biochem. Biotechnol., 18(1), 83–86.

33. Nagajyothi P.C., Sreekanth T.V.M., Tettey C.O., Jun Y.I., Mook S.H. 2014. Characterization, antibacterial, antioxidant, and cytotoxic activities of ZnO nanoparticles using *Coptidis* Rhizoma. Bioorg. Med. Chem. Lett., 24, 4298–4303.

34. Nwanya A.C., Razanamahandry L.C., Bashir A., Ikpo C.O., Nwanya S.C., Botha S., Ntwampe S.K.O., Ezema F.I., Iwuoha E.I., Maaza M.J. 2019. Industrial textile effluent treatment and antibacterial effectiveness of *Zea mays* L. Dry husk mediated bio-synthesized copper oxide nanoparticles.. Hazard Mater., 375, 281−289. https://doi.org/10.1016/j.jhazmat.2019.05.004

35. Obeidat M., Shatnawi M., Al-mazra'awi M.S., Al-Zu'bi, Al dmoor H, Al-Qudah, Qudah J., Otri I. 2012. Antimicrobial activity of crude extracts of some plant leaves. Res. J. Microbiol., 7(1), 59–67.

36. Pasiecznik N., Harris P.J., Smith S.J. 2004. Identifying tropical Prosopis species: a field guide. Hdra Publishing Coventry, UK.

37. Pillai A.M., Sivasankarapillai V.S., Rahdar A., Joseph J., Sadeghfar F.R., Anuf A., Kyzas K.R.G.Z. 2020. Green synthesis and characterization of zinc oxide nanoparticles ith antibacterial and antifungal activity. J. Mol. Struct., 1211, 128107.

38. Pradeep M., Kruszka D., Kachlicki P., Mondal D., Franklin G. 2022. Uncovering the phytochemical

basis and the mechanism of plant extract-mediated eco-friendly synthesis of silver nanoparticles using ultra-performance liquid chromatography coupled with a photodiode array and high-resolution mass spectrometry. ACS Sustain. Chem. Eng., 10, 562–571.

39. Raheem H.Q., Al-Thahab A., and Abd F.G. 2018. Antibacterial activity of silver nanoparticles extracted from *Proteus mirabilis* and healing the wound in rabbit. Biochem. Cell. Arch, 18(1), 97–104.

40. Rana S., Bajaj A., Mout R., Rotello V.M. 2012. Monolayer coated gold nanoparticles for delivery applications. Advanced drug delivery reviews 64, 200–216.

41. Rompre A., Servais P., Baudart J., De-Roubin M.-R., Laurent P. 2002. Detection and enumeration of coliforms in drinking water: current methods and emerging approaches. Journal of microbiological methods 49, 31–54.

42. Sangani M.H., Moghaddam M.N., Mahdi M. 2015. Inhibitory effect of zinc oxide nanoparticles on pseudomonas aeruginosa biofilm formation. Nanomed J., 2, 121–128.

43. Some S., Mondal R., Mitra D., Jain D., Verma D., Das S. 2021. Microbial pollution of water with special reference to coliform bacteria and their nexus with environment. Energy Nexus 1: 100008.

44. Sundrarajan M., Ambika S., Bharathi K. 2015. Plant-extract mediated synthesis of ZnO nanoparticlesusing Pongamia pinnata and their activity against pathogenic bacteria. Adv. Powder Technol., 26, 1294–1299.

45. Thukkaram M., Sitaram S., Kannaiyan S.K. 2014. Antibacterial Efficacy of Iron-Oxide Nanoparticles against Biofilms on Different Biomaterial Surfaces. Int J Biomater, 716080. https://doi.org/10.1155/2014/716080